Ocean Engineering 113 (2016) 57–63

Contents lists available at ScienceDirect

Ocean Engineering

journal homepage: www.elsevier.com/locate/oceaneng

Printed pressure housings for underwater applications

K. Breddermann [a,*], P. Drescher [b], C. Polzin [b], H. Seitz [b], M. Paschen [a]

[a] Chair of Ocean Engineering, University of Rostock, Albert-Einstein-Strasse 2, D-18059 Rostock, Germany
[b] Chair of Fluid Technology and Microfluidics, University of Rostock, Justus-von-Liebig-Weg 6, D-18059 Rostock, Germany

ARTICLE INFO

Article history:
Received 31 August 2015
Accepted 17 December 2015
Available online 9 January 2016

Keywords:
Pressure housings
Additive manufacturing
3D printing
Titanium
Ceramic

ABSTRACT

In order to investigate the capability of additive manufacturing technologies to build pressure housings, hemispheres made of titanium and ceramic with a nominal outer diameter of 70 mm were built on 3D printer systems, evaluated, and tested in a pressure tank. Titanium hemispheres expected to withstand an external pressure of 10 MPa started buckling at 6 MPa. A stiffened titanium hemisphere which was expected to withstand 24 MPa collapsed at 30 MPa. A ceramic hemisphere could not be tested to collapse since the measurement technique was not rated to withstand an external pressure above 30 MPa.

1. Introduction

Underwater vehicles used in deep-sea applications generally need pressure housings which have to withstand pressure loads up to 110 MPa in the water column. From an ocean engineer's point of view, it is a challenge to identify suitable materials as well as proper designs for pressure housings. The number of applicable and bearable solutions for extreme water depths is rather scarce worldwide. Additive manufacturing (AM) may lead to new solutions of these challenges.

In an AM process the desired object is built up by adding material layer by layer according to a three-dimensional CAD model. Developments over the past 20 years to improve additive manufacturing techniques have led to a shift in application from rapid prototyping to rapid manufacturing. Nowadays the application of AM products range from components fabricated for design verification, form and fit checking to end-use products capable to withstand highest loads. Materials presently used for AM are limited to a variety of metals, ceramics, polymers and resins. However, new materials are continuously developed. AM allows designs of complex-shaped parts which cannot be produced by common production processes like milling or turning (Fig. 1). Furthermore, the fabrication of complex single parts or small batches can be performed cost-effectively with AM (Guo and Leu, 2013).

In the overall design of an underwater vehicle many possibilities arise where additive manufacturing could be used to advantage: for example propellers or Kort nozzels (DEpagnier, 2007; Garvin et al., 2013) .

One of the major challenges for the designer of deep-sea underwater vehicles is to provide sufficient buoyancy of the vehicle in any water depth to compensate its weight. Sufficient buoyancy is a necessary prerequisite for a successful return of the vehicle to the water surface. In many cases, the designer is striving to achieve a so-called neutrally buoyant construction, i.e., the ratio of the weight of the vehicle to the weight of its displacement equals one. This ratio is often referred to as “the weight to displacement ratio”.

For each component of the vehicle and payload with a weight to displacement ratio greater than one, buoyancy elements have to be added by means of, e.g., buoyant syntactic foam or floatation spheres (Stevenson et al., 2003) to obtain a vehicle which is neutrally buoyant at total. With increasing water depth the weight to displacement ratio generally increases, since the wall thickness of the pressure housings and of the glass microspheres composing the syntactic foam (Weston et al., 2005) have to be increased in order to withstand the rising hydrostatic load. Hence, as (McDonald, 2013) noted, with heavier housings, greater floatation (with a larger weight to displacement ratio) is needed. The vehicle becomes bigger which (1) results in higher power requirements and which (2) might increase the vehicle size even further when batteries are used as energy source. Again, more floatation is needed and so on. The vehicle size increases non-linearly with the water depth and, as a final consequence, a larger ship for deployment is needed. Therefore, the primary design criterion is to develop the vehicle as light as possible and the pressure housings at the lowest possible weight to displacement ratio.

As mentioned above, additive manufacturing methods allow complex-shaped parts and enhance the freedom of the designer to

* Corresponding author.
E-mail address: karsten.breddermann2@uni-rostock.de (K. Breddermann).

http://dx.doi.org/10.1016/j.oceaneng.2015.12.033

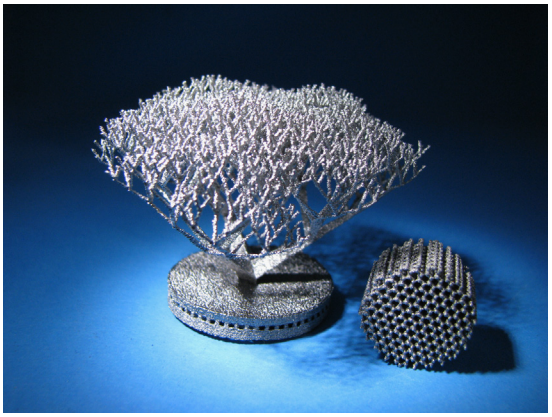

Fig. 1. Titanium structures fabricated in an electron beam melting process. The diameter of the base plate is 35 mm.

a yet unknown extent. Pressure housings with their penetration holes and joints might be fabricated with an optimal geometry and material usage according to the occurring stresses. Stiffeners could either be lightweight truss systems (Heinl et al., 2007; Cansizoglu et al., 2008; Quan et al., 2014) or inspired by bionic structures. The housings walls could be made of a thin outer shell supported by a space frame truss.

The ability to realise functional graded materials in an AM process (Guo and Leu, 2013), this means to build a material with gradually changing composition over volume and hence changing mechanical properties over volume, will further enhance the design possibilities. According to (Leu et al., 2012), even metal–ceramic combinations are in the scope of research to allow low-stress joints of graded ceramic parts and metal structures. These are just a few ideas beside many which may improve the weight to displacement ratio of pressure housings but they may show the newly attained freedom in designing. However, additive manufacturing processes are still developing and have to be improved. The dimensional accuracy, the surface quality and the material properties of the built parts may be critical parameters (Klocke et al., 2014; Lieneke et al., 2015) gave dimensional tolerances for several additive manufacturing processes and grouped additive manufacturing in the same tolerance classes as casting, drop forging and cutting. These machining processes will hardly achieve tolerances given for pressure housings in, for example, the rules for classification and construction of the Germanischer Lloyd Aktiengesellschaft (Ship Technology, 2009) to build unmanned underwater vehicles. Therefore, the aim of this paper is to report on the investigations of realizing printed pressure housings in titanium and ceramic, and to outline their challenges.

2. Material and methods

To investigate the capability of AM technologies, hemispheres made of titanium and ceramic were designed with a nominal outer diameter of 70 mm and calculated to withstand a nominal critical pressure of 10 MPa. The designs of the hemispheres had to be adapted to the limitations given by the AM processes and to allow a sealing to a camera pressure housing. After fabrication, the hemispheres were scanned to evaluate their dimensional accuracy and micrograph sections were taken from the titanium spheres to evaluate the material before they were then tested to collapse under external hydrostatic pressure.

2.1. Description of models

Fabrication of hemispheres of titanium: The titanium hemispheres were built with an electron beam melting (EBM) system A1 from the company Arcam AB, Sweden. In general, the EBM process has been established as a reproducible high quality manufacturing technology as shown in numerous publications (Heinl et al., 2007; Cansizoglu et al., 2008; Kahnert et al., 2007; Facchini et al., 2009; Koike et al., 2011). To build a part, a spherical titanium powder is spread out on a build plate and is selectively melted layer-wise by an electron beam into an almost fully dense material with a material porosity of 0.6% and a layer thickness of 70 µm. After the melting of a layer, the build plate is lowered by a step equal to one layer thickness, and another powder layer is spread out and then melted, and the process is repeated in order to obtain the three-dimensional part. A detailed description of the process is given in Kahnert et al. (2007).

The spherical titanium powder used is the Ti6Al4V alloy with a particle size distribution of 45–105 µm. For the design of the titanium hemispheres it is expected that the mechanical properties of the electron beam melted TI6Al4V are comparable to the wrought material and thus, a Young's modulus of 110 GPa, a Poisson's ratio of 0.3 and a yield strength of 828 MPa have been used for the design.

The wall thickness of the spheres is determined by the modified Zoelly–Van der Neut formula (Eq. 1) given in Sharp (1981)

$$p_e = 0.84 \cdot E\left(\frac{t}{r_{out}}\right)^2, \tag{1}$$

where p_e denotes the elastic buckling pressure, E the Young's modulus, t the wall thickness and r_{out} the outside radius of the sphere. This equation is valid for materials with a Poisson's ratio equal to 0.3. For the design purpose, it is expected that a failure will be due to elastic buckling, since a check of the wall thickness with the thin wall stress equation (Eq. 2) yielded to a thinner thickness to withstand the hydrostatic load of 10 MPa. In Eq. (2) r denotes the radius to the shell midsurface and σ the yield strength of the material. With the given design specifications a wall thickness of approximately 0.37 mm is obtained.

$$p_i = 2 \cdot \sigma \cdot \frac{t}{r} \tag{2}$$

However, the building process did not allow such a thin wall thickness and therefore the design wall thickness was set to 0.8 mm. In this case, an inelastic failure is expected, since the yield strength of the material is exceeded at 38 MPa, approximately 10 MPa less than the elastic buckling pressure. Close to the equator the wall thickness was increased to 3 mm to allow sealing to the camera housing with an O-Ring. The joint surface was ground. Furthermore, a stiffened variation was designed with a cylindrical section and a flange to clamp the hemispheres more easily to the camera housing. The technical sketches of the geometries are given in Fig. 2.

The second batch was designed with stiffeners 0.8 mm in width and 2.1 mm in height inside the hemisphere. A linear FEM analysis was done with ANSYS Mechanical 14 to estimate the collapse pressure of the stiffened hemisphere. The von Mises stress was used to define if the yield strength of the material was reached. As given in Fig. 3, the yield strength of the material (828 MPa) is exceeded at the run-out of the transition zone from flange to sphere at 23.9 MPa external pressure. Four hemispheres have been built from Batch 1 and two from Batch 2.

Fabrication of hemispheres of SiSiC ceramic: The ceramic hemispheres were built on a VX500 from the company voxeljet AG, Germany. The system was modified according to Polzin et al. (2015). The ceramic used is an experimental material still to be

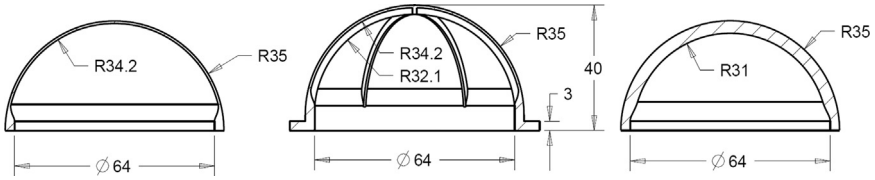

Fig. 2. Technical sketches of the hemispheres. From left to right: titanium hemisphere Batch 1, Batch 2, ceramic hemisphere.

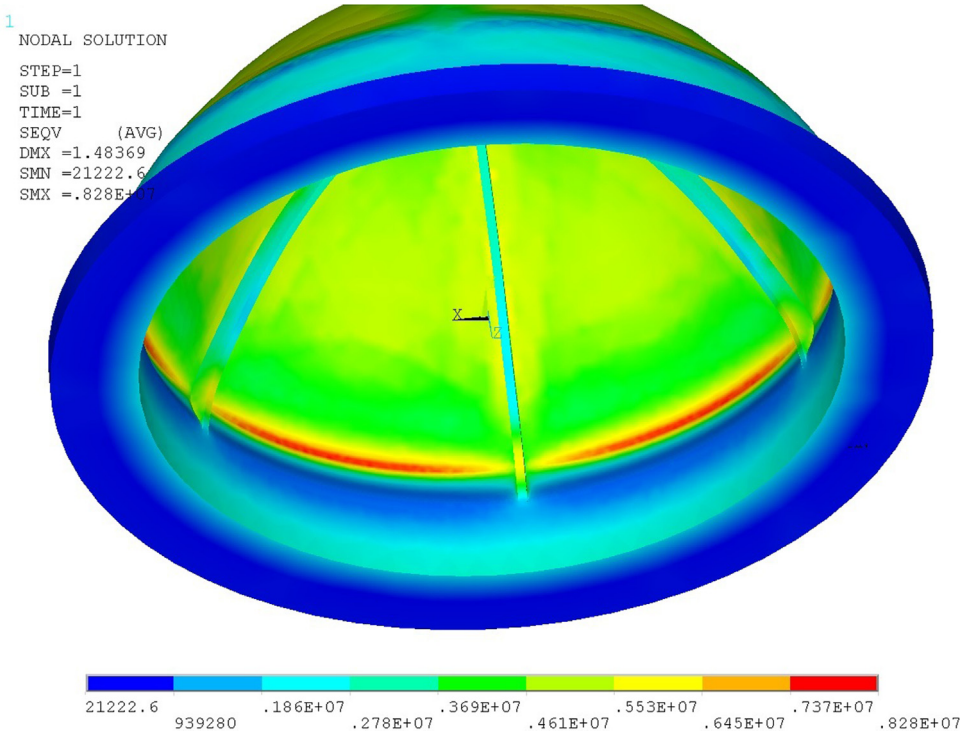

Fig. 3. Result of FEM analyse. Contour plot of von Mises stress.

improved by changing the composition of the constituent parts leading to a heat resistant material of high compressive strength. From the SiC ceramic powder a porous green part is produced layer by layer, with a layer thickness of approximately 100 µm. The green part is then infiltrated with Si in a thermal process, resulting in a fully dense part. The production process of the ceramic hemispheres is not yet fully mastered and the smallest wall thickness possible to produce was approximately 4 mm. The Youngs modulus, Poissons ratio and compressive strength used for the design of the SiSiC ceramic hemisphere are 14.8 GPa, 0.25, and 1345 MPa, respectively.

Since ceramics are brittle in nature, the deformation under load is elastic until failure Takagawa (2010). Therefore, the collapse pressure is determined by the Zoelly–Van der Neut formula, Eq. (3),

$$p_e = \frac{2 \cdot E}{\sqrt{3 \cdot (1-\nu^2)}} \cdot \left(\frac{t}{r}\right)^2 \tag{3}$$

where ν is the Poisson's ratio. The expected buckling pressure of the ceramic hemispheres is approximately 231 MPa. The yield strength is exceeded at 274 MPa. Surface processing to allow sealing with a camera housing was not practicable. Hence, the ceramic hemisphere was bonded to a joint ring made from alumina with epoxy adhesive.

Critical parameters: As mentioned in Introduction, the material properties, the dimensional accuracy and the surface quality of additive manufactured parts may be critical parameters. To quantify allowable deviations from the nominal geometry, the rules for classification and construction of the Germanischer Lloyd Ship Technology (2009) "Unmanned Submersibles (ROV, AUV) and Underwater Working Machines" are applied. Referring to these rules a deviation of the outer radius of $\pm$ 1% is acceptable. The out-of-roundness should not exceed $\pm$ 1% of the outer radius and the wall thickness should not fall below the nominal wall thickness. No information of an allowable surface roughness is given in this manual. The hemispheres tested by Krenzke and Kiernan (1965) to investigate the effect of initial imperfections were turned, which will give typically an averaged surface roughness R_a in the range of 0.4–6.3 µm. The material properties which are used for the design of the hemispheres are expected to be the lower limiting values. A deviation below these values is not acceptable.

According to the investigations concerning the dimensional accuracy published by Cooke and Soons (2010) and Lieneke et al. (2015), it is not clear if the requirements imposed by the classification rules can be met. Test parts produced for Cooke and Soons (2010) in an EBM process with dimensions in the order of the dimensions of the hemispheres showed deviations of the outer radius up to 0.6 mm, which is 50% more than the acceptable from the classification rules. The out-of-roundness with up to 0.35 mm is acceptable. Since the test parts were solid, no information about a wall thickness is given. The tolerance classes given by Lieneke et al. (2015) are rather broad. For the given hemispheres a range of tolerance of 0.2–1.9 mm has to be expected. The averaged surface roughness R_a of EBM manufactured parts ranges from approx. 20–30 µm (Safdar et al., 2012) which is comparable to the averaged surface roughness of hot rolled or sand casted parts and may

not be appropriate for pressure housings. The electron beam melted TI6Al4V typically has comparable mechanical properties to the wrought material, as Gong et al. (2012) summarized in their review article. However, Klocke et al. (2014) noted that the statistical confirmation of the material properties is still in the scope of current research.

The ceramic SiSiC material and its manufacturing process are also in the scope of current research. Hence, information about the critical parameters are not available in advance.

2.2. Test procedure

Before testing, the titanium hemispheres were scanned with a high-precision optical 3D scanning system. The system used was a GOM ATOS III (accuracy 0.005 mm, measuring point distance 0.07 mm). Furthermore, micrograph sections were taken from the titanium spheres to evaluate the material, the wall thickness and the surface quality in general. The surface roughness was not determined. Scans of the ceramic hemisphere were not carried out, since deviations to the expected geometry were visible to the naked eye.

Each hemisphere was tested in a 60 MPa rated pressure tank with an inner diameter of 1020 mm and 1500 mm depth. The pressure was read with a type 30 WIKA pressure sensor (accuracy 0.03 MPa). To observe the mode of failure, the hemisphere was coupled to a camera housing rated and tested up to 30 MPa (safety factor of 1.5). The set up is given in Fig. 4. A low-cost camera filmed the inside of the hemisphere until its collapse. For the next test, the camera and lighting were replaced. An analogous video signal was transmitted by wire to a PC, where the experiment was monitored in real-time and the received data were stored. The collapse was acoustically determined as well as indicated by a pressure drop in the pressure reading.

3. Results and discussion

In Figs. 5–7 the different hemispheres are depicted.

In order to build a reliable pressure housing in an AM process, it has to be ensured that the material properties throughout the part are homogeneous and that the dimensional accuracy of the part and the surface quality meet the requirements intended.

3.1. Evaluation

The polished micrograph in Fig. 8 shows a cutout close to the pole of a titanium hemisphere manufactured from Ti6Al4V powder in the EBM process. The EBM process leads to a microstructure better than cast Ti6Al4V, containing a lamellar α-phase with larger β-grains and with a higher density and significantly finer grain thanks to the rapid cooling of the melt pool (Facchini et al., 2009).

In Fig. 9 a microscope image is depicted of a cutout of a cross-section of the titanium hemispheres of Batch 1. The inside and outside surfaces are indicated by the white lines. Inspecting Fig. 9, three major problems become apparent:

1. *The surface quality is poor*: Failure under load will be promoted by notch effects. The surface quality results from powder particles sintering to the surfaces during the melting of the layers. Experiments from Karlsson et al. (2013) showed that the use of a material powder of smaller size will not improve the surface

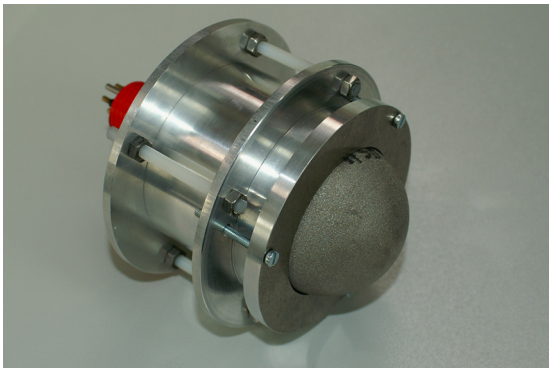

Fig. 4. The assembled pressure housing. The hemisphere, depicted in the right, joined to the camera housing.

Fig. 5. Titanium hemisphere of Batch 1.

Fig. 6. Titanium hemisphere of Batch 2 with the joint surface not yet ground.

Fig. 7. SiSiC ceramic hemisphere.

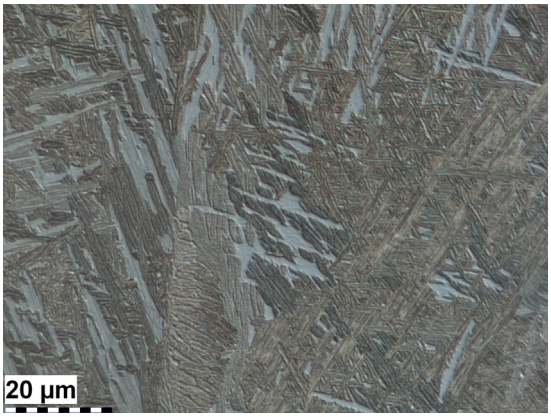

Fig. 8. Polished micrograph section. Cutout close to pole (1000 × magnification). Batch 1. Photo by Carola Ladewig.

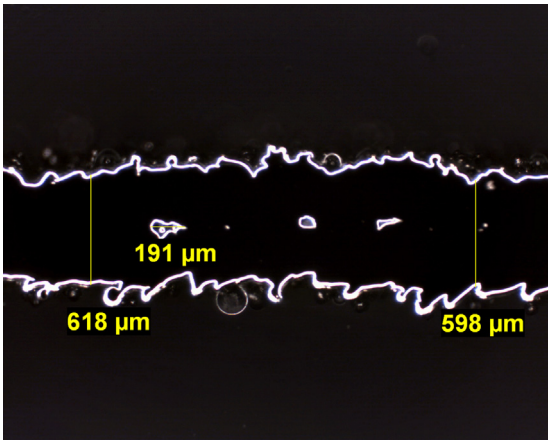

Fig. 9. Cutout of a cross-section (35 × magnification). The white lines indicating the inside and outside surfaces. Batch 1. Photo by Carola Ladewig.

quality at first but improvements may be possible by adjusting the melting process to the finer powder.

2. *The wall thickness varies*: Measurements at the cross-sections from a Batch 1 sphere registered wall thicknesses as thin as 0.38 mm, which is 48% of the nominal wall thickness. Cross-sections from a Batch 2 sphere showed deviations up to 15% from the nominal wall thickness. Smith et al. (2016) investigated reasons for undersized truss members and concluded that a too high energy input for melting adjacent layers which have little overlap to each other caused the inaccuracy. They could improve the dimensional accuracy (from −25% to +6 % deviation with regard to a cross-section area of a truss member) by adjusting the energy input for melting.
3. *Voids occur in the wall*: Voids in the material are supposed to originate from gas entrapments arising due to a too high energy input at melting (Gong et al., 2015) or from a lack of fusion due to a too low energy input (Smith et al., 2016). Thus, in order to minimize the voids, the energy input has to be adjusted. In addition, a hot isostatic pressuring (HIP) process may be carried out Al-Bermani et al. (2010) which will reduce the voids.

To get an overall impression of the dimensional accuracy, the 3D scans were evaluated. Presented in Figs. 10 and 11 is the deviation of the outer radius from the nominal radius. In Fig. 10, a titanium hemisphere of Batch 1 is given. Next to the pole a burr is visible which was removed before pressure testing. Around the pole an area is shown where the sphere is dented, a major imperfection which will weaken the hemisphere. Batch 1 was built

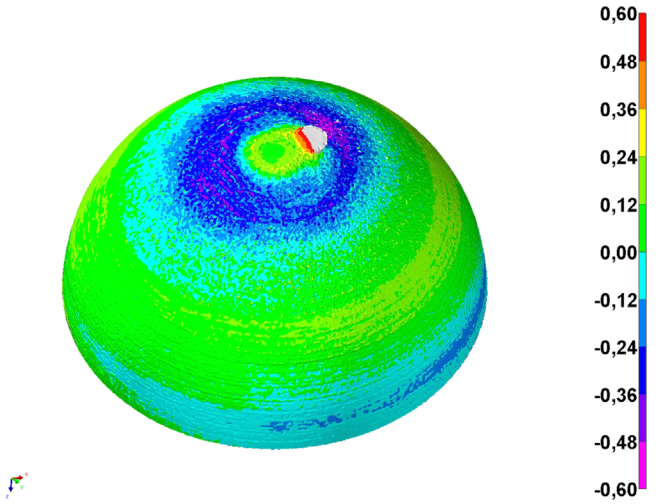

Fig. 10. Deviation in mm of the outer radius from the nominal radius of 35 mm. Batch 1.

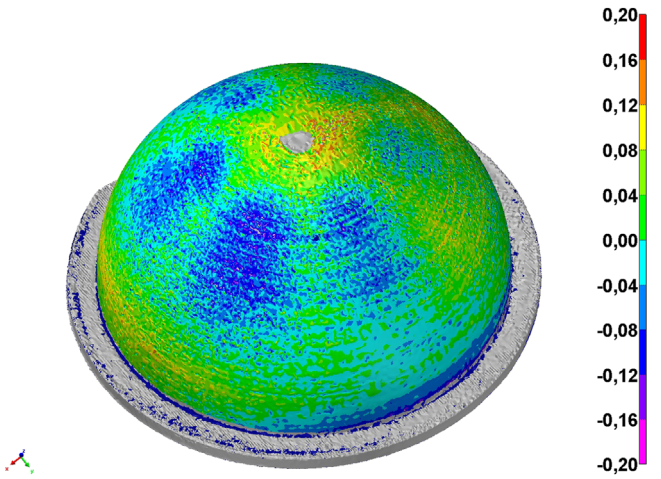

Fig. 11. Deviation in mm of the outer radius from the nominal radius. Batch 2.

up starting from the pole and it is assumed that due to the small contact area the melted material did not cool fast enough to support the ongoing building process of the sphere. Similar dents with similar dimensions could be observed on the other spheres of Batch 1. Two of the four hemispheres could not be used since the distortion broke open during the building process. Batch 2 (Fig. 11) was built up starting with the flange and with a support structure inside, which was removed after the building process. Due to this change the dimensional accuracy could be improved with the deviation of the radius ranging approximately from −0.2 mm to 0.2 mm, which corresponds to the given technical specification of the EBM system used.

However, both batches do not fulfil the specification given in the rules for classification and construction of the Germanischer Lloyd Ship Technology (2009). Batch 1 fails in all three categories. The deviation of the outer radius is up to 1.4%, the deviation of the out-of-roundness is up to 2.4% and the deviation of the wall thickness is 52%.

Batch 2 fails in the category wall thickness. The deviation of the outer radius is up to 0.4%, the deviation of the out-of-roundness is up to 0.8% and the deviation of the wall thickness is 15%. When inspecting Fig. 5 it can be noticed that the surface of the ceramic hemisphere shows various humps which developed during the infiltration process. Investigation of these humps showed accumulations of Si below a layer of SiSiC ceramic: an indication that

the amount of Si used for the infiltration was too large. To what extent these accumulations would influence the structural strength of the hemisphere could not be identified. The ceramic hemisphere is neither dimensionally accurate nor are its material properties consistent.

At this point it becomes apparent that major requirements imposed on the production method of a pressure housing cannot yet be achieved in an AM process. The surface quality is poor and requires further treatment to allow long-term operations. The material properties are homogeneous throughout the titanium parts, however, voids weaken the part. The material properties of the ceramic parts varied due to the accumulations of Si. Wall thickness and dimensional accuracy varied strongly for the titanium hemispheres of Batch 1 and the ceramic hemispheres. However, the dimensional accuracy of the titanium hemispheres of Batch 2 could be improved. As a consequence, a reliable prediction of the collapse pressure will hardly be possible, since the quality of the built hemispheres varies from specimen to specimen at this stage of development.

The improvements of Batch 2 have been achieved by changing the build direction and by using support structures. In the future, the energy input for melting the titanium powder has to be optimised to achieve a dimensional accurate part with a minimum of voids built in an EBM process (Gong et al., 2015; Smith et al., 2016). As long as this process parameter is not improved there is the need to further process the printed parts to ensure the dimensional accuracy and the surface quality expected for pressure housings. Near net shape parts could be produced and then machined to a given specification. However, this requires geometries which are producible with common manufacturing processes like milling or turning. The enhanced design freedom is lost. Nevertheless, it is to be checked if this is an effective production method for pressure housings, since the scrap material incurred can be reduced in comparison to common material removal methods. According to Klocke et al. (2014) it is a method applied for turbine blades.

Since the building process of the ceramic hemisphere is not yet fully mastered, future work will have to optimise the infiltration process in order to improve the material properties and to avoid the humps caused by the accumulations of Si. However, the experience and the knowledge gained from the infiltration process of the produced part will already allow modifications to achieve a housing with a thinner wall thickness and with improved material properties.

3.2. Experiment

A total of three specimens made from titanium have been tested to collapse: the two specimens remaining of Batch 1 and one of Batch 2. The pressure was increased by approx. 10 MPa every 20 min. In Table 1 the expected collapse pressure, the experimentally deduced collapse pressure and their deviation are summarised. The first hemisphere tested of Batch 1 started buckling at approx. 6.2 MPa and collapsed at approx. 6.9 MPa (Fig. 12). The second hemisphere started buckling at approx. 6.0 MPa and collapsed at approx. 7.1 MPa. As mentioned before, wall thicknesses as thin as 0.38 mm have to be expected. The predicted buckling pressure (Eq. 1) for this wall thickness of 0.38 mm is 10.9 MPa. With the mass of the hemispheres (32.2 g and 32.0 g) a nominal weight to displacement ratio of approx. 0.36 is obtained. If the joint region is not taken into account a ratio of 0.24 is achieved. The expected ratio of a near-perfect sphere at a collapse pressure of 6 MPa is 0.11 (mass calculation via Eq. 1). However, the geometry of the hemispheres of Batch 1 was dented around the pole and therefore the comparison to a near-perfect sphere may be not appropriate.

Table 1
Deviation of the experimentally deduced collapse pressure from the expected collapse pressure of the titanium hemispheres.

Hemisphere	Expected collapse pressure in MPa	Collapse pressure in MPa	Deviation
Batch 1	10.9	6.2	43
Batch 1	10.9	6.0	45
Batch 2	23.9	29.8	−25

The hemisphere of Batch 2 collapsed immediately at 29.8 MPa. Buckling could not be observed. Inspecting the remains of the sphere (Fig. 13) it is supposed that the FEM analysis predicted the failure region accurately. The failure load was underestimated. The yield strength of the material is already exceeded at a pressure of 23.9 MPa in the FEM analysis. However, as mentioned above, the dimensional accuracy varies and, as reported by Facchini et al. (2009), the yield strength might be better than that of the wrought material. The mass of the hemisphere with flange was 64.4 g, leading to a weight to displacement ratio of 0.57. Not taking the flange and the transition region with a mass of approx. 41 g into account, a weight to displacement ratio of 0.27 is obtained. The expected ratio (mass calculation via Eq. 2) of the not stiffened perfect sphere is 0.24. As noted above, the run-out of the transition region from flange to shell forms a predetermined breaking zone. This major design failure inhibited an even better performance of the stiffened hemisphere.

Fig. 12. Collapsed hemisphere of Batch 1.

Fig. 13. Collapsed hemisphere of Batch 2.

The ceramic hemisphere was tested up to 35 MPa without collapse. The test was stopped, since the camera housing was designed to withstand only 30 MPa with a safety factor of 1.5. Even though the pressure applied was just one seventh of the calculated collapse pressure and the weight to displacement ratio was 0.80 and therefore not competitive, the test is to be rated as a success. It was possible to show that 3D printed ceramic hemispheres made of SiSiC can be used for this kind of high pressure applications.

4. Conclusion

The investigations demonstrate that it is possible to build pressure housings in an additive manufacturing process. Although the number of tested specimens is too small to allow statements about the reliability of the housings and of the manufacturing process, nevertheless the test is apt to demonstrate that housings can be produced which feature a promising performance.

The work with AM machines bears new challenges, since the manufacturing process and the materials used are subjects of research themselves.

Since the dimensional accuracy and the surface finish achieved are predetermined by the AM process, the need arises to develop design criteria for reliable pressure housings which will suit the AM process. The benefit might be a far enhanced design freedom.

With the ability to realise extraordinary geometries made from a graded material with mechanical properties tailored to the occurring loads, a new kind of pressure housings with an enhanced weight to displacement ratio could be the future.

Acknowledgements

The authors wish to thank Carola Ladewig who took the microstructure sections, Fabian Gierschner who took the 3D scans, and Jannik Sobrado who assisted in carrying out the experiments.

References

Al-Bermani, S., Blackmore, M., Zhang, W., Todd, I., 2010. The origin of microstructural diversity, texture, and mechanical properties in electron beam melted Ti-6Al-4V. Metal. Mater. Trans. A 41 (13). http://dx.doi.org/10.1007/s11661-010-0397-x 3422–3434.

Cansizoglu, O., Harrysson, O., Cormier, D., West, H., Mahale, T., 2008. Properties of Ti-6Al-4V non385 stochastic lattice structures fabricated via electron beam melting. Mater. Sci. Eng. A 492 (1). http://dx.doi.org/10.1016/j.msea.2008.04.002 468–474.

Cooke A., Soons J., 2010. Variability in the geometric accuracy of additively manufactured test parts. In: 21st Annual International Solid Freeform Fabrication Symposium, Austin, Texas, USA, p. 1–12.

D'Epagnier, K.P., 2007. A computational tool for the rapid design and prototyping of propellers for underwater vehicles (Ph.D. thesis). Massachusetts Institute of Technology.

Facchini, L., Magalini, E., Robotti, P., Molinari, A., 2009. Microstructure and mechanical properties of Ti-6Al-4V produced by electron beam melting of pre-alloyed powders. Rapid Prototyping J. 15 (3). http://dx.doi.org/10.1108/13552540910960262 171–178.

Garvin M., Islam M., Molyneux D., Herrington P., 2013. The use of additive manufacturing techniques 395 in the construction of model-scale propellers. In: ASME 2013 32nd International Conference on Ocean, Offshore and Arctic Engineering. American Society of Mechanical Engineers. Article number V005T06A005. http://dx.doi.org/10.1115/OMAE2013-10088.

Gong X., Anderson T., Chou K., 2012. Review on powder-based electron beam additive manufacturing technology. In: ASME/ISCIE 2012 International Symposium on Flexible Automation. American Society of Mechanical Engineers, p. 507–515.

Gong H., Rafi K., Gu H., Ram G.J., Starr T., Stucker B., 2015. Influence of defects on mechanical properties of ti-6al-4v components produced by selective laser melting and electron beam melting. 400 Materials & Design 86, pp. 545–554. http://dx.doi.org/10.1016/j.matdes.2015.07.147.

Guo, N., Leu, M., 2013. Additive manufacturing: technology, applications and research needs. Front. 405 Mech. Eng. 8 (3). http://dx.doi.org/10.1007/s11465-013-0248-8 215–243.

Heinl, P., Rottmair, A., Körner, C., Singer, R.F., 2007. Cellular titanium by selective electron beam melting. Adv. Eng. Mater. 9 (5). http://dx.doi.org/10.1002/adem.200700025 360–364.

Kahnert M., Lutzmann S., Zaeh M., 2007. Layer formations in electron beam sintering. In: Solid freeform fabrication symposium, pp. 88–99.

Karlsson, J., Snis, A., Engqvist, H., Lausmaa, J., 2013. Characterization and comparison of materials produced by electron beam melting (ebm) of two different ti-6al-4v powder fractions. J. Mater. Process. Technol. 213 (12). http://dx.doi.org/10.1016/j.jmatprotec.2013.06.010 2109–2018.

Klocke, F., Klink, A., Veselovac, D., Aspinwall, D.K., Soo, S.L., Schmidt, M., Schilp, J., Levy, G., Kruth, J.P., 2014. Turbomachinery component manufacture by application of electrochemical, electro-physical and 415 photonic processes. CIRP Ann. Manuf. Technol. 63 (2). http://dx.doi.org/10.1016/j.cirp.2014.05.004 703–726.

Koike, M., Greer, P., Owen, K., Lilly, G., Murr, L.E., Gaytan, S.M., Martinez, E., Okabe, T., 2011. Evaluation of titanium alloys fabricated using rapid prototyping technologieselectron beam melting and laser beam melting. Materials 4 (10) 1776–1792.

Krenzke, M.A., Kiernan, T.J., 1965. Thes effect of initial imperfections on the collapse strength of deep spherical shells. Technical Report; DTIC Document.

Leu, M., Deuser, B.K., Tang, L., Landers, R.G., Hilmas, G., Watts, J.L., 2012. Freeze-form extrusion fabrication of functionally graded materials. CIRP Ann. Manuf. Technol. 61 (1). http://dx.doi.org/10.1016/j.cirp.2012.03.050 223–226.

Lieneke T., Adam G., Leuders S., Knoop F., Josupeit S., Delfs P., Funke N., Zimmer D., 2015. Systematical determination of tolerances for additive manufacturing by measuring linear dimensions. In: 26th Annual International Solid Freeform Fabrication Symposium, Austin, Texas, USA, p. 371–384.

McDonald, G., 2013. Operations to 11,000 m: Nereus ceramic housing design and analysis., OCEANS-San 430 Diego, IEEE, p. 1–5.

Polzin, C., Günther, D., Seitz, H., 2015. 3D printing of porous Al_2O_3 and *SiC* ceramics. J. Ceram. Sci. Technol. 6 (2), 141–146. http://dx.doi.org/10.4416/JCST2015-00013.

Quan, Y., Drescher, P., Zhang, F., Burkel, E., Seitz, H., 2014. Cellular ti6al4v with carbon nanotube-like structures fabricated by selective electron beam melting. Rapid Prototyping J. 20 (6) 541–550.

Safdar, A., He, H., Wei, L.Y., Snis, A., Chavez de Paz, L.E., 2012. Effect of process parameters settings and thickness on surface roughness of ebm produced ti-6al-4v. Rapid Prototyp. J. 18 (5), 401–408.

Sharp, A.G.,1981. Design curves for oceanographic pressure-resistant housings.

Rules for Classification and Construction, 2009. I Ship Technology, 5.3 Unmanned Submersibles (ROV, AUV) and Underwater Working Machines. Germanischer Lloyd Aktiengesellschaft.

Smith, C., Derguti, F., Nava, E.H., Thomas, M., Tammas-Williams, S., Gulizia, S., Fraser, D., Todd, I., 2016. Dimensional accuracy of electron beam melting (ebm) additive manufacture with regard to weight optimized truss structures. J. Mater. Process.Technol. 229, 128–138. http://dx.doi.org/10.1016/j.jmatprotec.2015.08.028.

Stevenson, P., Graham, D.,2003. Advanced materials and their influence on the structural design of AUVs. 445. In: Griffiths G. (ed.). Technology and applications of autonomous underwater vehicles. Abingdon: Taylor & Francis, p. 77–91.

Takagawa, S. New ceramic pressure hull design for deep water applications. In: OCEANS-Sydney, IEEE. p. 1–6. http://dx.doi.org/10.1109/OCEANSSYD.2010.5603796.

Weston, S., Stachiw, J., Merewether, R., Olsson, M., Jemmott, G., 2005. Alumina ceramic 3.6 in flotation 450 spheres for 11 km ROV/AUV systems. In: OCEANS-Washington, D.C IEEE, p. 172–177. http://dx.doi.org/10.1109/OCEANS.2005.1639757.18.